JACS
JOURNAL OF THE AMERICAN CHEMICAL SOCIETY

COMMUNICATION

pubs.acs.org/JACS

# Direct Synthesis of Spatially-Controlled Pt-on-Pd Bimetallic Nanodendrites with Superior Electrocatalytic Activity

Liang Wang,[†] Yoshihiro Nemoto,[†] and Yusuke Yamauchi*[,†,‡]

[†]World Premier International (WPI) Research Center for Materials Nanoarchitectonics (MANA), National Institute for Materials Science (NIMS), Namiki 1-1, Tsukuba, Ibaraki 305-0044, Japan

[‡]Precursory Research for Embryonic Science and Technology (PRESTO), Japan Science and Technology Agency (JST), 4-1-8 Honcho, Kawaguchi, Saitama 332-0012, Japan

Supporting Information

**ABSTRACT:** Here we report a facile synthesis of Pt-on-Pd bimetallic nanodendrites with a Pd interior and dendritic Pt exterior. The developed route rationally utilizes the spontaneous separation of the depositions of Pd and Pt, which endows direct formation of Pt-on-Pd nanodendrites. This is a truly simple and unique process that is quite different from the traditional seed-mediated growth strategy. Fine-tuning of the Pt and Pd ratios afforded Pt-on-Pd nanodendrites with superior electrocatalytic activity in comparison with commercial Pt electrocatalysts.

Currently, the tailored design of Pt-based bimetallic heteronanostructures has attracted considerable interest because these materials are highly promising catalysts.[1,2] In comparison with monometallic Pt nanostructures, Pt-based heteronanostructures show advanced catalytic activities.[3,4] For instance, relative to Pt alone, Pt−Au heteronanostructures show superior oxygen reduction activity.[5] The catalytic properties of the heteronanostructures are strongly dependent on their sizes, shapes, and compositions.[6−11] Fine control of the structural features and compositions is highly favorable for the creation of new Pt nanocatalysts with enhanced catalytic performance and improved Pt utilization efficiency.

Because of their superior catalytic activity, Pt−Pd heteronanostructures are among the most interesting metallic nanostructures.[12,13] They can be generally produced by either successive coreduction of Pt and Pd species[14−16] or a seed-mediated growth method.[17] For instance, hollow Pt−Pd alloyed nanocubes can be prepared by a coreduction route[16] and Pd@Pt core−shell nanoplates via the epitaxial growth of Pt on Pd nanoplates.[17] Among various Pt−Pd heteronanostructures, Pt-on-Pd bimetallic nanodendrites with highly branched shapes represent a very recently discovered new type of structure and are highly exciting electrocatalysts with high activity.[18,19] In contrast to traditional Pd@Pt core−shell structures, Pt-on-Pd nanodendrites with a small-sized Pd core and spatially separated Pt branches can drastically suppress the activity loss derived from the agglomeration of Pt active sites.

As a recent significant achievement, Pt-on-Pd nanodendrites were successfully prepared by a seed-mediated growth strategy using 9 nm octahedral Pd nanocrystals as seeds for the subsequent growth of Pt branches at 90 °C for 3 h, and they exhibited higher oxygen reduction activity than pure Pt.[18] Similar structures were also obtained by reducing $Pt(acac)_2$ in a diphenyl ether/oleylamine mixture in the presence of preformed 5 nm Pd nanoparticles as seeds under an argon atmosphere at 180 °C for 1 h.[19] To date, only very limited Pt-on-Pd nanodendrites have been demonstrated. Moreover, all of the previous reports have been based on seed-mediated growth strategies at high temperatures. Such two-step synthetic methods are strongly dependent on the use of faceted Pd seeds to direct the subsequent growth of the Pt branches.[18,19] Without the use of the preformed uniform and well-defined Pd seeds, both the particle size and shape of the Pt-on-Pd nanodendrites are uncontrollable.[18] Therefore, the development of a direct and effective route for large-scale synthesis is an urgent topic that must be addressed in order to further the evolution of the exciting and highly active Pt-on-Pd nanodendrites.

In this communication, we propose a very simple and high-yield route for the *direct* synthesis of Pt-on-Pd nanodendrites in aqueous solution at *room temperature* within 30 min *without* the need for any preformed Pd seeds, organic solvent, or high temperature. The newly developed one-step synthesis rationally utilizes the spontaneous separation of the depositions of Pd and Pt, resulting in the one-pot formation of Pt-on-Pd nanodendrites. By spatial control of both the composition and shape, superior electrocatalytic activity is realized. In contrast to the two-step seed-mediated growth strategies, the proposed method exhibits remarkable simplicity, which is a significant breakthrough in the synthesis of Pt-on-Pd nanodendrites.

To prepare Pt-on-Pd nanodendrites, 5 mL of an aqueous solution containing 17.5 mM $K_2PtCl_4$, 2.5 mM $Na_2PdCl_4$, and 1.74 mM Pluronic P123 (corresponding to $K_2PtCl_4$, $Na_2PdCl_4$, and Pluronic P123 amounts of 0.0875, 0.0125, and 0.0087 mmol, respectively) was placed in a small beaker. Next, 5 mL of 0.1 M ascorbic acid (AA) as a reducing agent was quickly added under stirring; after this addition, the final concentration of Pluronic P123 was 0.87 mM. The mixture was stirred for 30 min at room temperature. By consecutive washing/centrifugation cycles, the product was isolated and residual Pluronic P123 completely removed. The collected product was dried at 50 °C. The details of synthetic procedure are given in the Supporting Information.

Figure 1a shows TEM images of the as-prepared product. The product was found to consist of well-dispersed nanodendrites with complete dendritic shape, demonstrating the high-yield formation of nanodendrites (∼100%). The size of the nanodendrites narrowly ranged from 8 to 15 nm with an average diameter of 10 nm. This average size is notably smaller than the one

**Received:** March 31, 2011
**Published:** May 27, 2011





dx.doi.org/10.1021/ja202655j | J. Am. Chem. Soc. 2011, 133, 9674–9677

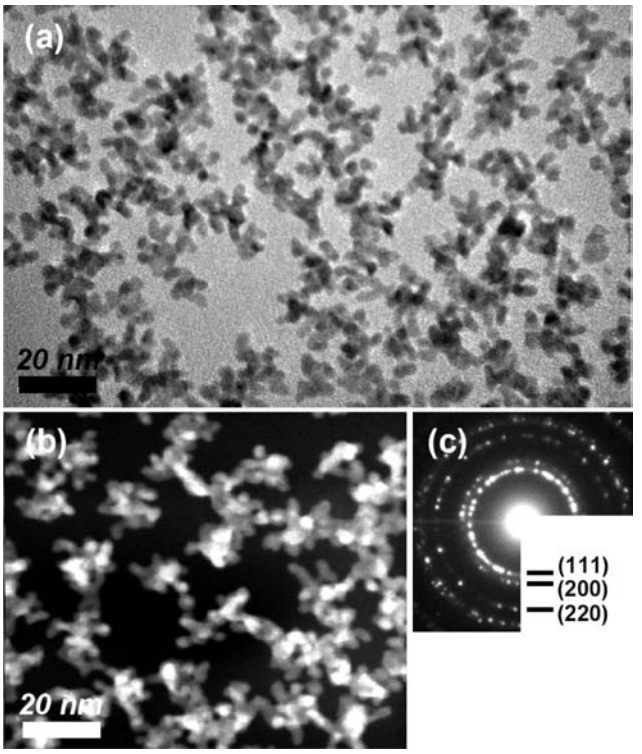


**Figure 1.** (a) Bright-field TEM image, (b) HAADF-STEM image, and (c) corresponding SAED pattern of the Pt-on-Pd bimetallic nanodendrites.

reported for nanodendrites prepared by using 9 nm Pd seeded growth (23.5 nm).[18] The dendritic nature of the product was further clearly visualized in a high-angle annular dark-field scanning TEM (HAADF-STEM) image (Figure 1b). The X-ray diffraction (XRD) profile of the nanostructures showed a metallic face-centered cubic (fcc) structure (Figure S1 in the Supporting Information), which was consistent with the selected-area electron diffraction (SAED) pattern (Figure 1c).

A highly magnified TEM image of one nanodendrite (Figure 2a) indicated that the nanoparticle was a dendritic entity having Pt nanoarms with widths of 3 nm branching in various directions. Nanoscale elemental mapping revealed that Pt was distributed throughout the entire nanodendrite (including the branches) and that Pd was concentrated in the core domain (Figure 2b). On the basis of the energy-dispersive X-ray spectroscopy (EDS) analysis of a single particle, the Pt/Pd atomic ratio was measured to be ~6.9/1.0. This value was in good agreement with the Pt/Pd atomic ratio in the initial reaction mixture (7.0/1.0), implying that all of the Pt and Pd precursors were completely reduced by AA. Random inspections further testified to the absence of isolated Pt and Pd nanostructures in the product. Thus, in all of the Pt-on-Pd nanodendrites, Pt branches were successfully coated onto the surfaces of Pd particles. Although similar Pt-on-Pd nanodendrites have been synthesized by two-step seed-mediated approaches,[18,19] the present one-step synthesis shows remarkable simplicity in comparison with them.

From Figure 2a, it was further noted that the Pt-on-Pd nanodendrite possessed well-developed crystallinity, and the observed lattice fringes were coherently extended over the entire nanodendrite. Because of the extremely high lattice match of Pt and Pd (99.23%),[18,19] no obvious grain boundaries between Pt

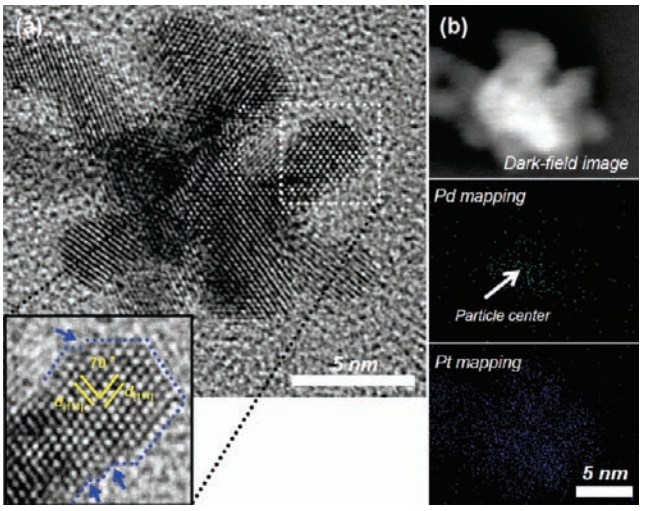


**Figure 2.** (a) Highly magnified TEM image and (b) corresponding EDS mapping images of one nanoparticle. The blue arrows in the inset of (a) indicate several atomic steps on the Pt branch surface.

and Pd were observed. Notably, each Pt branch was single-crystalline in nature. As shown in Figure 2a, both the observed *d* spacing (0.23 nm) for the adjacent fringes and the dihedral angle (70°) in the branch regions corresponded to the {111} planes of the Pt fcc structure. The single-crystalline nature of the Pt branches was caused by continuous Pt atomic addition on the Pd cores rather than by random aggregation of small Pt particles to form larger particles, for which twinning lattice fringes would have been clearly observed.[18,20]

The TEM results shown in Figure 2 revealed that the reduction of the Pd precursor by AA was preferentially performed before the Pt precursor reduction. The formed Pd nanoparticles served as in situ seeds for the subsequent deposition of Pt. During the later Pt deposition, Pluronic P123 supported the formation of the dendritic Pt exterior (Figure S2). The spontaneous separation of the Pd interior and the dendritic Pt exterior was caused by the different reduction kinetics of Pd and Pt complexes with AA. This was critical for the formation of the Pt-on-Pd nanodendrites.

It was importantly noted that several atomic steps were exposed on the Pt branch surface (Figure 2a), which can act as highly catalytic sites.[21−23] Notably, the Pt branches were spatially separated from each other, which was highly favorable for maximizing the Pt surface area. Analysis of the $N_2$ adsorption−desorption isotherm of the Pt-on-Pd nanodendrites gave a very high surface area of 48 $m^2\ g^{-1}$ (Figure S3). This value was ~2.2 times higher than that for a Pt black catalyst (~22 $m^2\ g^{-1}$). The Pt black was in a highly agglomerated form (Figure S4), while the Pt-on-Pd nanodendrites with spatially separated Pt branches were in an open dendritic form. Branching out was an effective way to fully improve the specific surface area of the catalysts. Furthermore, the rich edges and corner atoms derived from the branched Pt structures were highly valuable for enhancement of the Pt catalytic activity.[20]

While Pluronic P123 has been widely used as a typical mesostructural template for the synthesis of mesoporous silica and carbon,[24,25] it has very rarely been used for the synthesis of metallic nanostructures. In the present reaction system, the use of Pluronic P123 and the selected concentration were major factors in the high-quality formation of the Pt-on-Pd nanodendrites


dx.doi.org/10.1021/ja202655j |*J. Am. Chem. Soc.* 2011, 133, 9674–9677

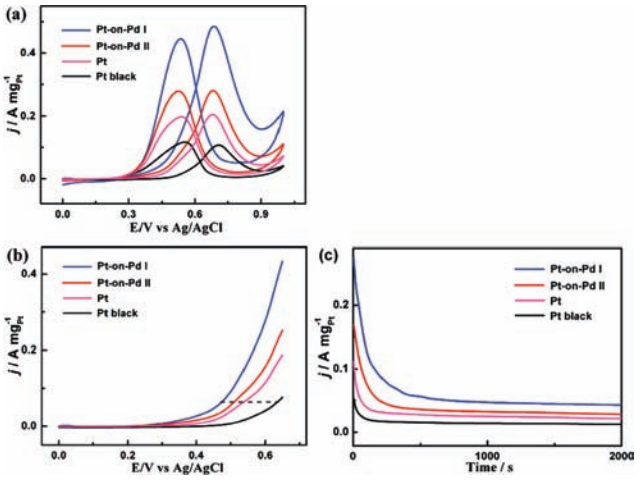


**Figure 3.** (a) Cyclic voltammograms, (b) linear-sweep voltammograms, and (c) chronoamperometric curves for methanol oxidation reactions catalyzed by Pt-on-Pd I (blue), Pt-on-Pd II (red), Pt nanodendrites without Pd cores (pink), and commercially available Pt black (black) in an aqueous solution containing 0.5 M $H_2SO_4$ and 1 M methanol. The chronoamperometric curves were recorded at 0.6 V. Pt-on-Pd I, Pt-on-Pd II, the Pt nanodendrites without Pd cores, and commercially available Pt black are displayed in Figure 1and Figures S7, S2a, and S4, respectively.

(Figures S5 and S6). Increasing the concentration of Pluronic P123 to 4.35 mM resulted in ill-defined dendritic nanoclusters (Figure S5a), and decreasing the Pluronic P123 concentration to 0.26 mM led to nanostructures in a highly aggregated form (Figure S5b). Replacing Pluronic P123 with Pluronic F68 resulted in highly aggregated nanoclusters (Figure S6a). Polyvinylpyrrolidone (PVP) is favorable for the formation of Pt-on-Pd nanodendrites in a seed-mediated strategy.[18] However, the use of PVP in the present reaction system resulted in irregular nanoparticles (Figure S6b). Interestingly, by simple control of the mole ratios of the Pt and Pd sources in the reaction solution, Pt-on-Pd nanodendrites with designed Pt and Pd ratios could be obtained (Figures S7 and S8). When the amounts of Pt and Pd sources were the same, the Pt/Pd atomic ratio in the product was 1.0/1.0, as revealed by EDS analysis of a single particle. In comparison with the shape displayed in Figure 1a, the dendritic nature of the product in Figure S7 was relatively decreased because of the increase in the Pd content, which was unfavorable for dendritic growth (Figure S2b). Such facile control of the dendritic nature in the Pt-on-Pd nanodendrites was highly valuable for tuning their catalytic properties.

Inspired by their attractive properties (e.g., dendritic Pt nanostructures with high surface area), we tested Pt-on-Pd nanodendrites with Pt/Pd atomic ratios of 6.9/1.0 (displayed in Figure 1 and denoted as Pt-on-Pd I) and 1.0/1.0 (displayed in Figure S7 and denoted as Pt-on-Pd II) as electrocatalysts for the methanol oxidation reaction (MOR). Their catalytic activities were further benchmarked against Pt nanodendrites without Pd cores (shown in Figure S2a) and commercially available Pt black (shown in Figure S4). The Pt-on-Pd nanodendrites exhibited better catalytic performance than either the Pt nanodendrites or Pt black (Figure 3). The mass-normalized current density of Pt-on-Pd I in the positive direction sweep [0.49 A (mg of Pt)$^{-1}$] was ~1.8 times higher than that of Pt-on-Pd II [0.28 A (mg of Pt)$^{-1}$], ~2.3 times higher than that of the Pt nanodendrites [0.21 A (mg of Pt)$^{-1}$], and ~4.5 times higher than that of Pt black [0.11 A (mg of Pt)$^{-1}$] (Figure 3a). Furthermore, at any oxidation current density (e.g., as indicated by the dashed line in Figure 3b), the corresponding oxidation potentials on the Pt-on-Pd nanodendrites were obviously lower than those on the Pt nanodendrites and Pt black, further suggesting that the methanol oxidation reaction was easier to perform on the Pt-on-Pd nanodendrites. Chronoamperometric curves recorded at 0.6 V for 2000 s (Figure 3c) indicated that the current densities of the Pt-on-Pd nanodendrites were higher than those of Pt nanodendrites and Pt black over the entire time range.

In comparison with Pt black (Figure S4), the open dendritic structure of the Pt-on-Pd nanodendrites is highly beneficial for their use as an electrocatalyst, primarily because of their superior tolerance to undesirable agglomeration of the active sites. The presence of the Pd core in each Pt-on-Pd nanodendrite not only facilitates the growth of the Pt branches but also plays a key role in the enhanced activity of the Pt-on-Pd nanodendrites relative to pure Pt nanodendrites. The atoms of Pd and Pt are highly miscible, and the Pd atoms in the core domain coherently match with the lattice structures of the exterior Pt branches (Figure 2a and Figure S8a), resulting in the formation of the inserted pseudo-Pd−Pt alloy heterointerface,[26] which is favorable for reducing the electronic binding energy in Pt and facilitating the C−H cleavage reaction in methanol decomposition.[27] Furthermore, the many atomic steps exposed on the Pt branch surface (Figure 2a) can act as highly active sites for the MOR.[21−23] Thus, superior catalytic activity was realized through the open dendritic structure with the designed Pt and Pd ratios.

In summary, we have developed a very simple and efficient route for the direct and high-yield synthesis of Pt-on-Pd bimetallic nanodendrites with designed Pt and Pd ratios. The bimetallic heteronanostructures with Pd interior and dendritic Pt exterior were synthesized by spontaneous step-by-step depositions of Pd and Pt precursors. In comparison with the reported two-step seed-mediated approaches, the present rational design is highly valuable because it extraordinarily simplifies the synthesis of the exciting Pt-on-Pd bimetallic nanostructures. We expect that the developed rational block copolymer-mediated synthesis will in the future trigger the facile creation of novel multimetallic heteronanostructures with designed compositions and desired properties.

## ■ ASSOCIATED CONTENT

**Ⓢ Supporting Information.** Experimental details and additional characterization data. This material is available free of charge via the Internet at http://pubs.acs.org.

## ■ AUTHOR INFORMATION

**Corresponding Author**
Yamauchi.Yusuke@nims.go.jp

## ■ ACKNOWLEDGMENT

L.W. greatly appreciates the JSPS for support in the form of a fellowship tenable at NIMS.

## ■ REFERENCES

(1) Chen, A. C.; Holt-Hindle, P. *Chem. Rev.* **2010**, *110*, 3767–3804.
(2) Peng, Z. M.; Yang, H. *Nano Today* **2009**, *4*, 143–164.

(3) (a) Guo, S. J.; Dong, S. J.; Wang, E. K. *ACS Nano* **2010**, *4*, 547–555. (b) Guo, S. J.; Dong, S. J.; Wang, E. K. *Chem. Commun.* **2010**, *46*, 1869–1871.
(4) Yang, H. Z.; Zhang, J.; Sun, K.; Zou, S. Z.; Fang, J. Y. *Angew. Chem., Int. Ed.* **2010**, *49*, 6848–6851.
(5) Kim, Y.; Hong, J. W.; Lee, Y. W.; Kim, M.; Kim, D.; Yun, W. S.; Han, S. W. *Angew. Chem., Int. Ed.* **2010**, *49*, 10197–10201.
(6) Liu, Z. F.; Jackson, G. S.; Eichhorn, B. W. *Angew. Chem., Int. Ed.* **2010**, *49*, 3173–3176.
(7) Wu, J. B.; Zhang, J. L.; Peng, Z. M.; Yang, S. C.; Wagner, F. T.; Yang, H. *J. Am. Chem. Soc.* **2010**, *132*, 4984–4985.
(8) Xu, D.; Bliznakov, S.; Liu, Z. P.; Fang, J. Y.; Dimitrov, N. *Angew. Chem., Int. Ed.* **2010**, *49*, 1282–1285.
(9) Zhang, J.; Yang, H. Z.; Fang, J. Y.; Zou, S. Z. *Nano Lett.* **2010**, *10*, 638–644.
(10) Kang, Y. J.; Murray, C. B. *J. Am. Chem. Soc.* **2010**, *132*, 7568–7569.
(11) Kim, J.; Lee, Y.; Sun, S. H. *J. Am. Chem. Soc.* **2010**, *132*, 4996–4997.
(12) Lim, B.; Xia, Y. N. *Angew. Chem., Int. Ed.* **2011**, *50*, 76–85.
(13) (a) Habas, S. E.; Lee, H.; Radmilovic, V.; Somorjai, G. A.; Yang, P. D. *Nat. Mater.* **2007**, *6*, 692–697. (b) Lee, H.; Habas, S. E.; Somorjai, G. A.; Yang, P. D. *J. Am. Chem. Soc.* **2008**, *130*, 5406–5407.
(14) (a) Lim, B.; Wang, J. G.; Camargo, P. H. C.; Cobley, C. M.; Kim, M. J.; Xia, Y. N. *Angew. Chem., Int. Ed.* **2009**, *48*, 6304–6308. (b) Yuan, Q.; Zhou, Z. Y.; Zhuang, J.; Wang, X. *Chem. Commun.* **2010**, *46*, 1491–1493.
(15) Wang, L.; Yamauchi, Y. *Chem.—Asian J.* **2010**, *5*, 2493–2498.
(16) Huang, X. Q.; Zhang, H. H.; Guo, C. Y.; Zhou, Z. Y.; Zheng, N. F. *Angew. Chem., Int. Ed.* **2009**, *48*, 4808–4812.
(17) Lim, B.; Wang, J. G.; Camargo, P. H. C.; Jiang, M. J.; Kim, M. J.; Xia, Y. N. *Nano Lett.* **2008**, *8*, 2535–2540.
(18) Lim, B.; Jiang, M. J.; Camargo, P. H. C.; Cho, E. C.; Tao, J.; Lu, X. M.; Zhu, Y. M.; Xia, Y. N. *Science* **2009**, *324*, 1302–1305.
(19) Peng, Z. M.; Yang, H. *J. Am. Chem. Soc.* **2009**, *131*, 7542–7543.
(20) Mahmoud, M. A.; Tabor, C. E.; El-Sayed, M. A.; Ding, Y.; Wang, Z. L. *J. Am. Chem. Soc.* **2008**, *130*, 4590–4591.
(21) Zhou, Z. Y.; Huang, Z. Z.; Chen, D. J.; Wang, Q.; Tian, N.; Sun, S. G. *Angew. Chem., Int. Ed.* **2010**, *49*, 411–414.
(22) Tian, N.; Zhou, Z. Y.; Sun, S. G.; Ding, Y.; Wang, Z. L. *Science* **2007**, *316*, 732–735.
(23) Lee, S. W.; Chen, S.; Sheng, W. C.; Yabuuchi, N.; Kim, Y.; Mitani, T.; Vescovo, E.; Shao-Horn, Y. *J. Am. Chem. Soc.* **2009**, *131*, 15669–15677.
(24) Wan, Y.; Zhao, D. Y. *Chem. Rev.* **2007**, *107*, 2821–2860.
(25) Song, L. Y.; Feng, D.; Fredin, N. J.; Yager, K. G.; Jones, R. L.; Wu, Q. Y.; Zhao, D. Y.; Vogt, B. D. *ACS Nano* **2010**, *4*, 189–198.
(26) Yamauchi, M.; Kobayashi, H.; Kitagawa, H. *ChemPhysChem* **2009**, *10*, 2566–2576.
(27) Liu, L.; Pippel, E.; Scholz, R.; Gosele, U. *Nano Lett.* **2009**, *9*, 4352–4358.